Optical Engineering

OpticalEngineering.SPIEDigitalLibrary.org

Topology optimization of support structure of multiwaveband imaging system

Xiaohu Li
Ming Xuan
Junlin Ma
Liming Zheng
Qiang Sun
He Wang

SPIE.

Optical Engineering 54(11), 115113 (November 2015)

Topology optimization of support structure of multiwaveband imaging system

Xiaohu Li,[a,b,*] Ming Xuan,[a] Junlin Ma,[a] Liming Zheng,[a] Qiang Sun,[a] and He Wang[a]
[a]Chinese Academy of Science, Changchun Institute of Optics, Fine Mechanics and Physics, Department of Photoelectric Technology, No. 3888, Dongnanhu Road, Changchun 130033, China
[b]University of Chinese Academy of Sciences, Beijing 100039, China

Abstract. It is shown by a prototype experiment that the deformation of a support structure leads to relative deflection of the optical axes of a multiwaveband imaging system and then inconsistency of the fields of view of the subsystems. To solve this issue, a topology optimization method with the objective of minimizing the deflection angles of the optical axes is proposed. The method consists of the establishment of a deflection angle equation, the construction of an objective function, and the achievement of optimization using commercial software. Then, a new optimization structure is extracted from the topology optimization model. The comparative analysis between the original structure and the optimization structure shows that the deflection angles of the optical axes after topology optimization decrease greatly, which proves the effectiveness of the proposed method. [DOI: 10.1117/1.OE.54.11.115113]

Keywords: multiwaveband; support structure; relative shift of fields of view; deflection of the optical axes; topology optimization.

Paper 151150 received Aug. 28, 2015; accepted for publication Oct. 27, 2015; published online Nov. 30, 2015.

1 Introduction

In order to maintain the consistency of the fields of view (FOVs) of the subsystems of a multiwaveband imaging system,[1–4] image registration usually needs to be used. To some extent, the bigger the relative shift of FOV is, the larger the search range in the image registration process. This implies that more calculation amount of image registration is required. Therefore, for the purpose of reducing computation burden and raising efficiency of image registration, improving the parallelism (or perpendicularity) of the optical axes[5,6] forms an important part in the structural design of the imaging system. When several optomechanical units are assembled on the same support structure, the deformation of the support structure caused by self-weight, external forces, or other factors will lead to relative deflection of the optical axes and inconsistency of the FOV. To meet the rigidity requirement, the topology optimization of the support structure in order to decrease the relative deflection of optical axes appears to be very necessary.

Topology optimization is an efficient way to acquire new configurations during the concept design stage, and it is widely used in many optomechanical structure fields. Weidong et al.[7] optimized the support structure of telescope skin in a multiobjective way to decrease the weight, and to improve the flexibility for in-plane morphing and the ability to resist out-of-plane pressure. Xia et al.[8] used the level set method to optimize the continuum structure and support forms with the aim of reducing the flexibility. Richardson et al.[9] used the volume fraction as constraint to optimize the truss structure with the aim of reducing the weight and flexibility. Yinjun et al.[10] optimized the weight and rigidity of a space camera support structure. It can be seen that scholars used flexibility, rigidity, weight, and volume as objective functions to accomplish the topology optimization. So far, no topology optimization with the aim of decreasing the relative deflection of optical axes has been reported. Furthermore, commercial software such as HyperWorks® and Natran® cannot respond to the change of deflection of the optical axes directly. Thus, in order to take the deflection angle of the optical axes as an optimization objective, it is necessary to use built-in responses of commercial software to establish the relation equations of the deflection angle by geometric transformation and then construct the objective function.

In this paper, topology optimization for the support structure of a multiwaveband imaging system is implemented with the objective of decreasing the deflection angles of the optical axes, thus obtaining the topological configurations. Then a new structure, which can be practically applied, is extracted from the optimization model. Finally, a comparative analysis between the optimization structure and the original structure is conducted.

2 Prototype Experiment

The optomechanical structure of the multiwaveband imaging system, which can obtain images of target in the near-infrared (NIR), visible (RGB), and ultraviolet (UV) wavebands simultaneously, is shown in Fig. 1. The operational principle of this system is described as follows. First, the incident beam is split into three different waveband beams by cemented prisms. Then, one of the three beams goes directly through the corresponding lens groups, and the other two go through the corresponding lens groups after being reflected by the reflectors. Finally, the three beams are captured by charge-coupled device (CCD) cameras, and the finial images are obtained. Some parameters of this system are shown in Table 1.

*Address all correspondence to: Xiaohu Li, E-mail: 282105186@qq.com

0091-3286/2015/$25.00

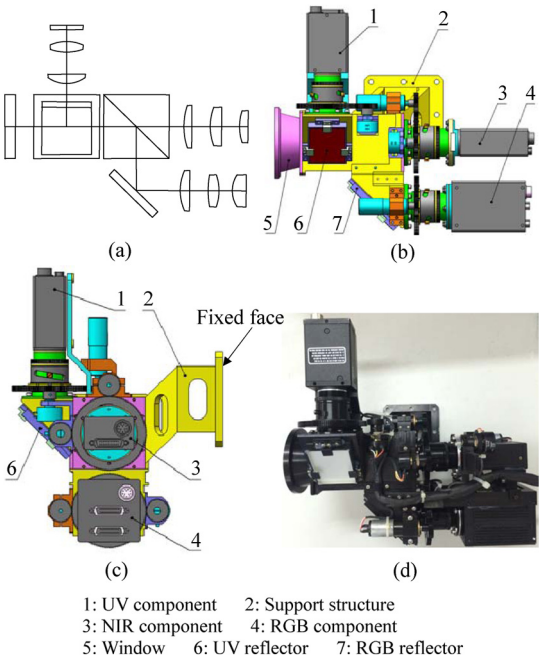

Fig. 1 Optomechanical structure of the multiwaveband imaging system: (a) schematic of optical structure, (b) right view of mechanical structure, (c) back view of mechanical structure, and (d) the principle prototype.

Table 1 Some parameters of this imaging system.

	Ultraviolet (UV)	Visible (RGB)	Near-infrared (NIR)
Waveband	0.3 to 0.4 μm	0.4 to 0.76 μm	0.76 to 1.1 μm
Field of view	7.4 × 5.5 deg	7.4 × 5.5 deg	7.4 × 5.5 deg
Focal length	50 mm	50 mm	50 mm
F#	4	4	4
Spatial resolution	≤0.2 mrad	≤0.2 mrad	≤0.2 mrad

This imaging system is a part of an integrated reconnaissance system, which contains several other types of imaging and radar equipment. The data processing of the integrated system is a computationally intensive task. In order to reduce the calculation amount of image registration and enhance the ability of real-time scout, the relative shift of FOV of this imaging system should be <2 pixels.

Considering the limitation of space and weight, as well as the convenience of assembly and adjustment, the optomechanical components, including the cemented prisms and the reflectors, were all installed on the same support structure. In Fig. 1(c), the side face of the support structure is fixed, which makes it similar to a cantilever beam. This structural type has a characteristic of low rigidity, so the relative shift of FOV may occur due to the mechanical deformation. Unfortunately, it is verified in the optical alignment and experiment process of a principle prototype [as shown in Fig. 1(d)].

The specific method of the optical alignment is as follows. An electrical cross-target is generated in the center of each CCD. The window of the prototype is aligned with a collimator with cross-hair reticule. By adjusting the position of the prototype, make sure that the electrical cross of NIR CCD coincides with the cross-hair of the collimator. Then, the shift between the electrical cross of visible CCD and the cross-hair of the collimator could be observed. So is the shift between the electrical cross of UV CCD and the cross-hair of the collimator. Through careful lapping and adjustment, it is possible for us to make the shift of FOV <0.6 pixels, which can meet the requirement.

In order to facilitate the alignment and adjustment, an auxiliary tool needs to be used in the whole process of optical alignment. The use of the auxiliary tool leads to the support structure being under the situation of unloading because the auxiliary tool bears all loads at this time. However, under normal operating condition, there is no auxiliary tool and the support structure bears all loads. The normal operating condition of the support structure is different from the optical alignment condition, which may result in the change of FOV.

The images, taken by the principle prototype under normal operating condition, are shown in Fig. 2. The pixel coordinates of points A, B, and C were acquired in the three different waveband images, and the results are shown in Table 2. It can be seen with the NIR waveband image as a benchmark that the visible waveband image has an average shift of ~2.3 pixels with a maximum of 3 pixels, and the UV waveband image has an average shift of ~2.7 pixels with a maximum of 4 pixels. Obviously, the relative shift of FOV becomes larger. Then, the reason is discussed carefully. The auxiliary tool has little impact on the relative shift of FOV in the optical alignment process. The most important difference is the load state of the support structure after optical alignment. Thus, we believe it is the deformation of the support structure that leads to the change of FOV.

In order to verify this opinion further, a static structural analysis of the simplified imaging system was conducted, as shown in Fig. 3. The forces F_1, F_2, F_3, and F_4 are the

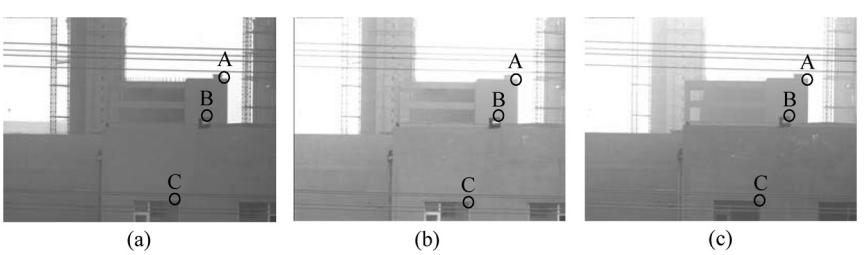

Fig. 2 Three waveband images taken by the prototype: (a) near-infrared image, (b) visible image, and (c) ultraviolet image.

Table 2 Pixel coordinate values of points A, B, and C in the three waveband images.

	A		B		C	
	X	*Y*	*X*	*Y*	*X*	*Y*
NIR	725	199	667	321	568	598
RGB	723	202	666	323	565	601
UV	722	201	665	323	564	601
RGB-NIR	−2	3	−1	2	−3	3
UV-NIR	−3	2	−2	2	−4	3

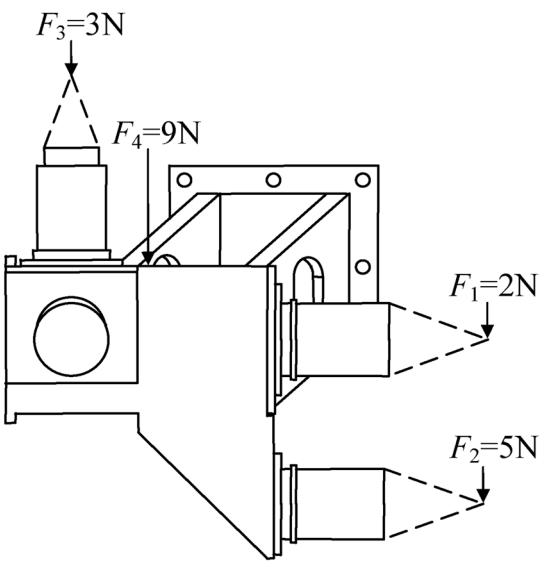

Fig. 3 Static structural analysis of the system.

weight of the NIR subsystem, visible subsystem, UV subsystem, and prismatic components, respectively. The analysis results show that the maximum deformation of the support structure is 9.9 μm, and the optical axes of visible subsystem and UV subsystem deflect ~27 and 35″, respectively (details are described in Table 2). According to the focal length ($f = 50$ mm) and the pixel size ($l = 4.65$ μm), the relative shift of FOV caused by the mechanical deformation of the support structure can be calculated, which is ~1.4 and 1.8 pixels, respectively. Obviously, this cannot be ignored.

There are two ways to solve this problem. One is to change the optical alignment method. Make sure that the optical alignment condition of the support structure is the same as the normal operating condition. The other is to increase the rigidity of the support structure by topology optimization. Then, the shift of FOV will not change too much after the optical alignment. Through careful consideration, we decide to choose the second way because it is easy to implement.

3 Optimization Elements

Optimization design elements consist of design variables, objective function, and constraint conditions.[11–13] The objective function is the function about the design variables. Also, the design domain needs to be considered for practical application.

3.1 *Selecting the Design Domain*

The support structure is shown in Fig. 4. Referring to Fig. 1, the optomechanical components of the UV, NIR, and visible subsystems are assembled in areas 1 to 3, respectively. Area 5 is for a fixed connection, and thus it cannot be used as an optimization area. Area 4 is the cantilever part of the support structure, which has an important impact on rigidity, so it is selected as the design domain.

3.2 *Determining Constraint Conditions*

The system has a strict limitation on weight, so the weight is considered a constraint condition. However, the weight constraint can be turned into a volume fraction constraint, because all the components are made of the same material (in another word, with the same density), so volume fraction constraint is used in the optimization. Details are described in Sec. 5.

3.3 *Constructing an Objective Function*

The purpose of topology optimization is to decrease the deflection of the optical axes and maintain the consistency of the FOV. However, commercial software cannot directly provide the response of the deflection angle, so the displacement responses of the endpoints of the optical axes need to be used to establish the equation of the deflection angle of the optical axes by geometric transformation. Then, the objective function can be constructed.

4 Objective Function

In order to maintain the consistency of the FOV, we need to decrease the relative deflection angle of the optical axes rather than the absolute deflection angle. There are two possible ways to bring about the relative deflection between optical axes of different waveband subsystems. One is the direct deflection by structural deformation. The other is by deflection of reflectors as the result of structural deformation, which causes the indirect deflection of the optical axes.

The methods of solving these two conditions vary because of different principles. With the first condition, the angles between the deformed optical axes need to be calculated directly. For the second condition, the absolute deflection angles of the reflectors need to be calculated first. The relative deflection angles between the optical axes can then be obtained according to the reflection law,

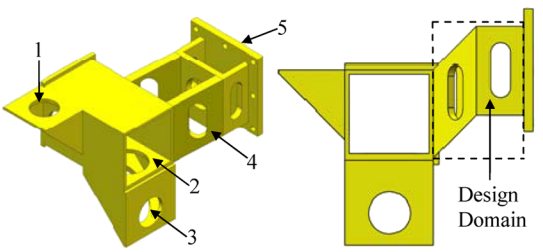

Fig. 4 Support structure and design domain.

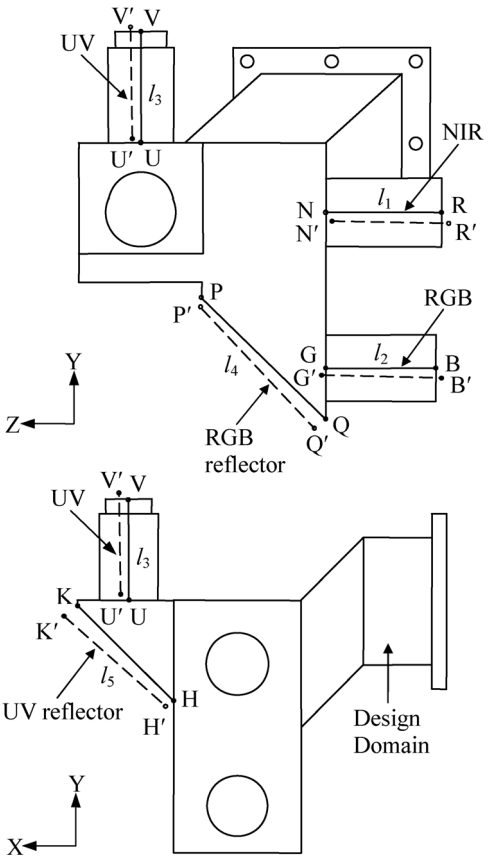

Fig. 5 Deflection of the optical axes.

which will be twice as much as the deflection angles of the reflectors.

As shown in Fig. 5, the optical axes of the NIR subsystem, visible subsystem, and UV subsystem are denoted as NR, GB, and UV, respectively, with their lengths (distance from the first lens to the last) denoted as l_1, l_2, and l_3, respectively. After the deformation, the optical axes deflect to N′R′, G′B′, and U′V′. In order to simplify the calculation, the optical axes are considered to be straight lines despite the possible distortion. Likewise, the RGB and UV reflectors are simplified to two lines in the same plane with their corresponding optical axes PQ and KH (lengths as l_4 and l_5), respectively. After the deformation, the reflectors deflect to P′Q′ and K′H′, respectively.

Here are several settings under the initial condition:

1. The optical axes of the NIR subsystem and the visible subsystem are mutually parallel (NR‖GB), and optical axes of the NIR subsystem and the UV subsystem are mutually perpendicular (NR ⊥ UV).
2. The plane formed by NR and GB is set as the YZ plane, and the direction of X axis is determined by the right-hand rule.
3. The angle between line PQ and Y axis is 45 deg, and the angle between line KH and Y axis is also 45 deg.

The following content is the computational procedures of the relative deflection angles formed by the optical axes under the two conditions mentioned earlier. Then, the objective function is constructed.

4.1 *Structural Deformation*

According to the settings given above, the endpoint coordinates of three optical axes can be defined as

$$\begin{aligned}
&\mathrm{N} = (0, y_1, z_1), \quad \mathrm{R} = (0, y_1, z_1 - l_1)\\
&\mathrm{G} = (0, y_2, z_2), \quad \mathrm{B} = (0, y_2, z_2 - l_2)\\
&\mathrm{U} = (x_3, y_3, z_3), \quad \mathrm{V} = (x_3, y_3 + l_3, z_3).
\end{aligned} \tag{1}$$

In the formula above, $y_1, z_1, \ldots, y_3$, and z_3 represent the coordinate values of the corresponding endpoints in directions X, Y, and Z, respectively.

The endpoint coordinates after deformation are

$$\begin{aligned}
\mathrm{N}' &= (\Delta x_{\mathrm{N}}, y_1 + \Delta y_{\mathrm{N}}, z_1 + \Delta z_{\mathrm{N}})\\
\mathrm{R}' &= (\Delta x_{\mathrm{R}}, y_1 + \Delta y_{\mathrm{R}}, z_1 - l_1 + \Delta z_{\mathrm{R}})\\
\mathrm{G}' &= (\Delta x_{\mathrm{G}}, y_2 + \Delta y_{\mathrm{G}}, z_2 + \Delta z_{\mathrm{G}})\\
\mathrm{B}' &= (\Delta x_{\mathrm{B}}, y_2 + \Delta y_{\mathrm{B}}, z_2 - l_2 + \Delta z_{\mathrm{B}})\\
\mathrm{U}' &= (x_3 + \Delta x_{\mathrm{U}}, y_3 + \Delta y_{\mathrm{U}}, z_3 + \Delta z_{\mathrm{U}})\\
\mathrm{V}' &= (x_3 + \Delta x_{\mathrm{V}}, y_3 + l_3 + \Delta y_{\mathrm{V}}, z_3 + \Delta z_{\mathrm{V}}).
\end{aligned} \tag{2}$$

In the formula above, $\Delta x_{\mathrm{R}}, \Delta y_{\mathrm{R}}, \Delta z_{\mathrm{R}}, \ldots, \Delta y_{\mathrm{V}}$, and Δz_{V} represent the offsets of the corresponding endpoints in directions X, Y, and Z, respectively.

Vectors of optical axes after deformation can be obtained as follows:

$$\begin{aligned}
\overrightarrow{\mathrm{N}'\mathrm{R}'} &= (\Delta x_{\mathrm{NR}}, \Delta y_{\mathrm{NR}}, -l_1 + \Delta z_{\mathrm{NR}})\\
\overrightarrow{\mathrm{G}'\mathrm{B}'} &= (\Delta x_{\mathrm{GB}}, \Delta y_{\mathrm{GB}}, -l_2 + \Delta z_{\mathrm{GB}})\\
\overrightarrow{\mathrm{U}'\mathrm{V}'} &= (\Delta x_{\mathrm{UV}}, l_3 + \Delta y_{\mathrm{UV}}, \Delta z_{\mathrm{UV}}),
\end{aligned} \tag{3}$$

where $\Delta x_{\mathrm{NR}} = \Delta x_{\mathrm{R}} - \Delta x_{\mathrm{N}}$, $\Delta y_{\mathrm{NR}} = \Delta y_{\mathrm{R}} - \Delta y_{\mathrm{N}}$, $\Delta z_{\mathrm{NR}} = \Delta z_{\mathrm{R}} - \Delta z_{\mathrm{N}}$, and so on.

In order to calculate the deflection angles of the optical axes, the angle formula between two space vectors[14] is commonly used, which can be described as follows:

$$\begin{aligned}
\cos\angle(\overrightarrow{\mathrm{N}'\mathrm{R}'}, \overrightarrow{\mathrm{G}'\mathrm{B}'}) &= \frac{\overrightarrow{\mathrm{N}'\mathrm{R}'} \cdot \overrightarrow{\mathrm{G}'\mathrm{B}'}}{|\overrightarrow{\mathrm{N}'\mathrm{R}'}||\overrightarrow{\mathrm{G}'\mathrm{B}'}|}\\
\cos\angle(\overrightarrow{\mathrm{N}'\mathrm{R}'}, \overrightarrow{\mathrm{U}'\mathrm{V}'}) &= \frac{\overrightarrow{\mathrm{N}'\mathrm{R}'} \cdot \overrightarrow{\mathrm{N}'\mathrm{R}'}}{|\overrightarrow{\mathrm{N}'\mathrm{R}'}||\overrightarrow{\mathrm{U}'\mathrm{V}'}|}.
\end{aligned} \tag{4}$$

However, it is noticed that variables such as Δx_{NR}, Δy_{NR}, and Δz_{NR} are four to five orders of magnitude smaller than l_1, l_2, and l_3. When significant digits involved in the calculation are not enough or the round-off error is large, small numbers will be overwhelmed by larger numbers.[15] This leads to the loss of calculation accuracy and poor results for the topology optimization. Thus, Eq. (4) needs to be replaced by a new equivalent function.

Normalizing the vectors of the optical axes, we have

$$\begin{aligned}
\overrightarrow{j_{N'R'}} &= \frac{\overrightarrow{N'R'}}{|\overrightarrow{N'R'}|} \approx \left(\frac{\Delta x_{NR}}{l_1}, \frac{\Delta y_{NR}}{l_1}, -1 + \frac{\Delta z_{NR}}{l_1}\right) \\
\overrightarrow{j_{G'B'}} &= \frac{\overrightarrow{G'B'}}{|\overrightarrow{G'B'}|} \approx \left(\frac{\Delta x_{GB}}{l_2}, \frac{\Delta y_{GB}}{l_2}, -1 + \frac{\Delta z_{GB}}{l_2}\right) \\
\overrightarrow{j_{U'V'}} &= \frac{\overrightarrow{U'V'}}{|\overrightarrow{U'V'}|} \approx \left(\frac{\Delta x_{UV}}{l_3}, 1 + \frac{\Delta y_{UV}}{l_3}, \frac{\Delta z_{UV}}{l_3}\right) \\
|\overrightarrow{j_{N'R'}}| &= |\overrightarrow{j_{G'B'}}| = |\overrightarrow{j_{U'V'}}| = 1.
\end{aligned} \tag{5}$$

Figure 6 shows the angle formed by the normalized vectors of the optical axes, $\overrightarrow{j_{N'R'}}$ and $\overrightarrow{j_{G'B'}}$. The angle is very small, and the norms of the two vectors are equal, so $\theta_1 = \theta_2 \approx 90$ deg. According to the Sine theorem,[14] we have

$$\begin{aligned}
\sin\angle(\overrightarrow{j_{N'R'}}, \overrightarrow{j_{G'B'}}) &= \frac{|\overrightarrow{j_{G'B'}} - \overrightarrow{j_{N'R'}}| \sin\theta_2}{|\overrightarrow{j_{G'B'}}|} = |\overrightarrow{j_{G'B'}} - \overrightarrow{j_{N'R'}}| \\
&= \sqrt{(\Delta x_{12})^2 + (\Delta y_{12})^2 + (\Delta z_{12})^2},
\end{aligned} \tag{6}$$

where

$$\begin{aligned}
\Delta x_{12} &= \frac{\Delta x_{GB}}{l_2} - \frac{\Delta x_{NR}}{l_1} \\
\Delta y_{12} &= \frac{\Delta y_{GB}}{l_2} - \frac{\Delta y_{NR}}{l_1} \\
\Delta z_{12} &= \frac{\Delta z_{GB}}{l_2} - \frac{\Delta z_{NR}}{l_1}.
\end{aligned}$$

It can be seen that Δx_{12}, Δy_{12}, and Δz_{12} are all small, with nearly the same order of magnitude. This avoids the unacceptable case mentioned earlier.

$\overrightarrow{j_{U'V'}}$ and $\overrightarrow{j_{N'R'}}$ in Fig. 5 are approximately mutually perpendicular. To maintain the consistency of the calculation, we rotated $\boldsymbol{j}_{U'V'}$ along X axis clockwise by 90 deg to create vector $\boldsymbol{j}_{UVX}$. Then, $\sin\angle(\boldsymbol{j}_{N'R'}, \boldsymbol{j}_{U'V'})$ was replaced by $\sin\angle(\boldsymbol{j}_{N'R'}, \boldsymbol{j}_{UVX})$, yielding

$$\begin{aligned}
\overrightarrow{j_{UVX}} &\approx \left(\frac{\Delta x_{UV}}{l_3}, \frac{\Delta z_{UV}}{l_3}, -1 - \frac{\Delta y_{UV}}{l_3}\right) \sin\angle(\overrightarrow{j_{N'R'}}, \overrightarrow{j_{UVX}}) \\
&= |\overrightarrow{j_{UVX}} - \overrightarrow{j_{N'R'}}| = \sqrt{(\Delta x_{13})^2 + (\Delta y_{13})^2 + (\Delta z_{13})^2},
\end{aligned} \tag{7}$$

where

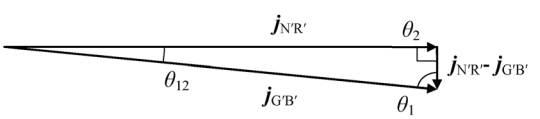

Fig. 6 Angle between vectors of the optical axes.

$$\begin{aligned}
\Delta x_{13} &= \frac{\Delta x_{UV}}{l_3} - \frac{\Delta x_{NR}}{l_1} \\
\Delta y_{13} &= \frac{\Delta z_{UV}}{l_3} - \frac{\Delta y_{NR}}{l_1} \\
\Delta z_{13} &= -\frac{\Delta y_{UV}}{l_3} - \frac{\Delta z_{NR}}{l_1}.
\end{aligned}$$

4.2 *Reflector Deflection*

The endpoint coordinates of the reflectors can be defined as

$$\begin{aligned}
P &= (x_4, y_4, z_4), \quad Q = \left(x_4, y_4 - \frac{l_4}{\sqrt{2}}, z_4 - \frac{l_4}{\sqrt{2}}\right) \\
K &= (x_5, y_5, z_5), \quad H = \left(x_5 - \frac{l_5}{\sqrt{2}}, y_5 - \frac{l_5}{\sqrt{2}}, z_5\right).
\end{aligned} \tag{8}$$

The endpoint coordinates after deformation are

$$\begin{aligned}
P' &= (x_4 + \Delta x_P, y_4 + \Delta y_P, z_4 + \Delta z_P) \\
Q' &= \left(x_4 + \Delta x_Q, y_4 - \frac{l_4}{\sqrt{2}} + \Delta y_Q, z_4 - \frac{l_4}{\sqrt{2}} + \Delta z_Q\right) \\
K' &= (x_5 + \Delta x_K, y_5 + \Delta y_K, z_5 + \Delta z_K) \\
H' &= \left(x_5 - \frac{l_5}{\sqrt{2}} + \Delta x_H, y_5 - \frac{l_5}{\sqrt{2}} + \Delta y_H, z_5 + \Delta z_H\right).
\end{aligned} \tag{9}$$

Similarly, $\Delta x_P, \Delta y_P, \Delta z_P, \ldots, \Delta y_H$, and Δz_H represent the offsets of the corresponding endpoints in directions X, Y, and Z, respectively.

The reflector vectors can be obtained as

$$\overrightarrow{PQ} = \left(0, -\frac{l_4}{\sqrt{2}}, -\frac{l_4}{\sqrt{2}}\right) \qquad \overrightarrow{KH} = \left(-\frac{l_5}{\sqrt{2}}, -\frac{l_5}{\sqrt{2}}, 0\right). \tag{10}$$

The reflector vectors after deformation can be obtained as

$$\begin{aligned}
\overrightarrow{P'Q'} &= \left(\Delta x_{PQ}, \Delta y_{PQ} - \frac{l_4}{\sqrt{2}}, \Delta z_{PQ} - \frac{l_4}{\sqrt{2}}\right) \\
\overrightarrow{K'H'} &= \left(\Delta x_{KH} - \frac{l_5}{\sqrt{2}}, \Delta y_{KH} - \frac{l_5}{\sqrt{2}}, \Delta z_{KH}\right),
\end{aligned} \tag{11}$$

where $\Delta x_{PQ} = \Delta x_P - \Delta x_Q$, $\Delta y_{PQ} = \Delta y_P - \Delta y_Q$, and so on.

The reflector vectors after normalization are

$$\begin{aligned}
\overrightarrow{j_{PQ}} &= \frac{\overrightarrow{PQ}}{|\overrightarrow{PQ}|} = \left(0, -\frac{1}{\sqrt{2}}, -\frac{1}{\sqrt{2}}\right) \\
\overrightarrow{j_{KH}} &= \frac{\overrightarrow{KH}}{|\overrightarrow{KH}|} = \left(-\frac{1}{\sqrt{2}}, -\frac{1}{\sqrt{2}}, 0\right) \\
\overrightarrow{j_{P'Q'}} &= \frac{\overrightarrow{P'Q'}}{|\overrightarrow{P'Q'}|} \approx \left(\frac{\Delta x_{PQ}}{l_4}, \frac{\Delta y_{PQ}}{l_4} - \frac{1}{\sqrt{2}}, \frac{\Delta z_{PQ}}{l_4} - \frac{1}{\sqrt{2}}\right) \\
\overrightarrow{j_{K'H'}} &= \frac{\overrightarrow{KH}}{|\overrightarrow{K'H'}|} \approx \left(\frac{\Delta x_{KH}}{l_5} - \frac{1}{\sqrt{2}}, \frac{\Delta y_{KH}}{l_5} - \frac{1}{\sqrt{2}}, \frac{\Delta z_{KH}}{l_5}\right).
\end{aligned} \tag{12}$$

The absolute deflection angles of the reflectors can be obtained as

$$\sin\angle(\overrightarrow{j_{PQ}},\overrightarrow{j_{P'Q'}}) = |\overrightarrow{j_{P'Q'}} - \overrightarrow{j_{PQ}}| = \sqrt{\left(\frac{\Delta x_{PQ}}{l_4}\right)^2 + \left(\frac{\Delta y_{PQ}}{l_4}\right)^2 + \left(\frac{\Delta z_{PQ}}{l_4}\right)^2}, \tag{13}$$

$$\sin\angle(\overrightarrow{j_{KH}},\overrightarrow{j_{K'H'}}) = |\overrightarrow{j_{K'H'}} - \overrightarrow{j_{KH}}| = \sqrt{\left(\frac{\Delta x_{KH}}{l_5}\right)^2 + \left(\frac{\Delta y_{KH}}{l_5}\right)^2 + \left(\frac{\Delta z_{KH}}{l_5}\right)^2}. \tag{14}$$

4.3 *Objective Function*

According to the above description, the deflection angle of the optical axis of the visible subsystem with respect to that of NIR subsystem, δ_1, can be obtained as

$$\delta_1 = \angle(\overrightarrow{j_{N'R'}},\overrightarrow{j_{G'B'}}) + 2\angle(\overrightarrow{j_{PQ}},\overrightarrow{j_{P'Q'}}) = \arcsin\left[\sqrt{(\Delta x_{12})^2 + (\Delta y_{12})^2 + (\Delta z_{12})^2}\right] + 2\arcsin\left[\sqrt{\left(\frac{\Delta x_{PQ}}{l_4}\right)^2 + \left(\frac{\Delta y_{PQ}}{l_4}\right)^2 + \left(\frac{\Delta z_{PQ}}{l_4}\right)^2}\right]. \tag{15}$$

Similarly, the deflection angle of the UV subsystem, δ_2, can be obtained as

$$\delta_2 = \angle(\overrightarrow{j_{N'R'}},\overrightarrow{j_{U'V'}}) + 2\angle(\overrightarrow{j_{KH}},\overrightarrow{j_{K'H'}}) = \arcsin\left[\sqrt{(\Delta x_{13})^2 + (\Delta y_{13})^2 + (\Delta z_{13})^2}\right] + 2\arcsin\left[\sqrt{\left(\frac{\Delta x_{KH}}{l_5}\right)^2 + \left(\frac{\Delta y_{KH}}{l_5}\right)^2 + \left(\frac{\Delta z_{KH}}{l_5}\right)^2}\right]. \tag{16}$$

The aim of this optimization is to minimize δ_1 and δ_2 simultaneously, which involves the following two problems.

1. Calculation of δ_1 and δ_2 directly by Eqs. (15) and (16) will lead to excessive calculation due to the antitrigonometric function and square root operation. Thus, the formulas need to be simplified.
2. The optimization of two deflection angles at the same time forms a multiobjective issue, which needs to be turned into a single-objective issue.[16,17]

Because the arc-sin function is a monotone function, the following approximation in a minizone is valid:

$$\min(\delta_1) \Leftrightarrow \min\left[\sqrt{(\Delta x_{12})^2 + (\Delta y_{12})^2 + (\Delta z_{12})^2}\right] + 2\min\left[\sqrt{\left(\frac{\Delta x_{PQ}}{l_4}\right)^2 + \left(\frac{\Delta y_{PQ}}{l_4}\right)^2 + \left(\frac{\Delta z_{PQ}}{l_4}\right)^2}\right], \tag{17}$$

$$\min(\delta_2) \Leftrightarrow \min\left[\sqrt{(\Delta x_{13})^2 + (\Delta y_{13})^2 + (\Delta z_{13})^2}\right] + 2\min\left[\sqrt{\left(\frac{\Delta x_{KH}}{l_5}\right)^2 + \left(\frac{\Delta y_{KH}}{l_5}\right)^2 + \left(\frac{\Delta z_{KH}}{l_5}\right)^2}\right]. \tag{18}$$

To remove the square-root calculation, the weighted square sum method is used to turn it into a single-objective problem.[18] Then, the objective function $f(i)$ can be defined as

$$f(i) = (\Delta x_{12})^2 + (\Delta y_{12})^2 + (\Delta z_{12})^2 + (\Delta x_{13})^2 + (\Delta y_{13})^2 + (\Delta z_{13})^2 + 2\left[\left(\frac{\Delta x_{PQ}}{l_4}\right)^2 + \left(\frac{\Delta y_{PQ}}{l_4}\right)^2 + \left(\frac{\Delta z_{PQ}}{l_4}\right)^2\right] + 2\left[\left(\frac{\Delta x_{KH}}{l_5}\right)^2 + \left(\frac{\Delta y_{KH}}{l_5}\right)^2 + \left(\frac{\Delta z_{KH}}{l_5}\right)^2\right]. \tag{19}$$

5 Optimization Result

The whole topology optimization procedure is operated on the module HyperMesh, OptiStruct, and HyperView of the commercial software HyperWorks. OptiStruct is a powerful optimization solver. It adopts mathematical programming method, constructs approximate model by solving the sensitivity, and obtains optimal solution by using small-step iterative. Specific steps are described below.

1. Import the three-dimensional model into HyperMesh, mesh the model, create the materials and properties, and then assign them to each component: The finite element model of the topology optimization is shown in Fig. 7. It consists of the support structure and three lens cones, all of which are made of aluminum alloy with the following mechanical properties: elastic modulus E of 68 GPa, Poisson's ratio v of 0.33, and density ρ of 2700 kg/m^3.
2. Apply force boundary condition: As with the static structural analysis in Fig. 3, the weights of the NIR subsystem, visible subsystem, and UV subsystem (F_1, F_2, and F_3) are applied on the corresponding lens cones, respectively. The weights of prisms, reflectors, and other parts (F_4) are applied on the support structure as a concentrated load, as shown in Fig. 7.
3. Apply constraint boundary condition: The fixed constraint boundary is set on the side of the support structure, as shown in Fig. 7.
4. Create load step: Combine the force and constraint boundary conditions mentioned earlier in a load step.

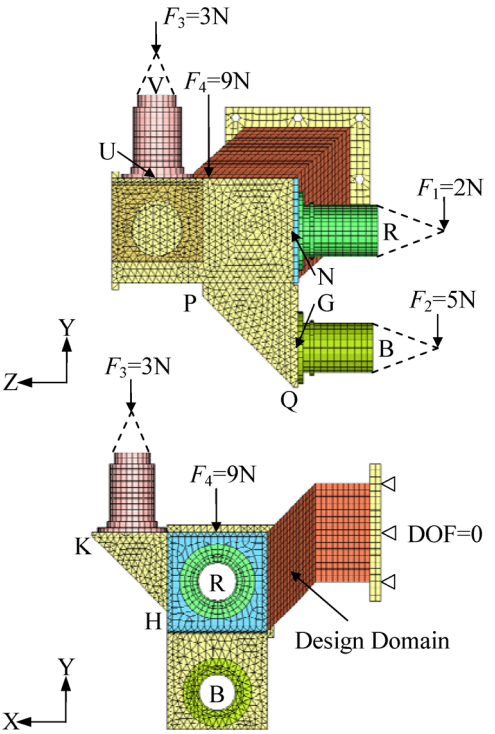

Fig. 7 Finite element model of the topology optimization.

5. Define design variable: Element density of each element of the design domain, as shown in Fig. 7, is set as design variable automatically by the software. The design domain has 13,311 elements, while the whole finite element model has 47,689 elements. The number of elements is proper for the optimization.
6. Define optimization objective: This step consists of three substeps.
   a. Create 30 displacement responses from ten points (N, R, G, B, U, V, P, Q, K, and H), and each point has three coordinate directions.
   b. Establish function response based on Eq. (19).
   c. Set function response as the optimization objective.
7. Define optimization constraint: This step consists of two substeps.
   a. Create volume fraction response. Details are described in Sec. 3.2.
   b. Set volume fraction response as optimization constraint and assign value to it. The original structure is light-weighted. As compared to the original structure, the weight should not be increased. Thus, the optimization constraint is set to be <0.4.
8. Implement optimization calculation and check optimization results through HyperView. The iterative curve of the objective function in Fig. 8 shows a convergent optimization process: OptiStruct takes element density of each element in the design domain as design variable. The value range of element density is 0.0 to 1.0. If element density of an element is close to 1.0 that means the element is important and it needs to be preserved. If element density of an element is close to 0.0, it can be removed. In HyperView, the different topology optimization models can be obtained by adjusting element density. The optimization model with element density of 0.25 is shown in Fig. 9. The element density of 0.25 is chosen, because those preserved elements (element density > 0.25) constitute the main features of the topology structure and also the requirement of light-weighted is well met. It can be seen from Fig. 9 that the optimization structure mainly consists of two transverse plates (1 and 2) and one vertical plate (3), forming a semiclosed structure on the back side. Among these three plates, the shape of plate 1 is very irregular, the thickness is not even, and the machinability is not well either. Relatively, the shapes of plates 2 and 3 are more

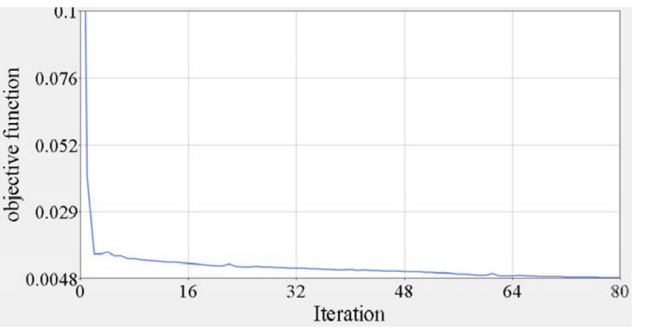

Fig. 8 Iterative curve of the objective function.

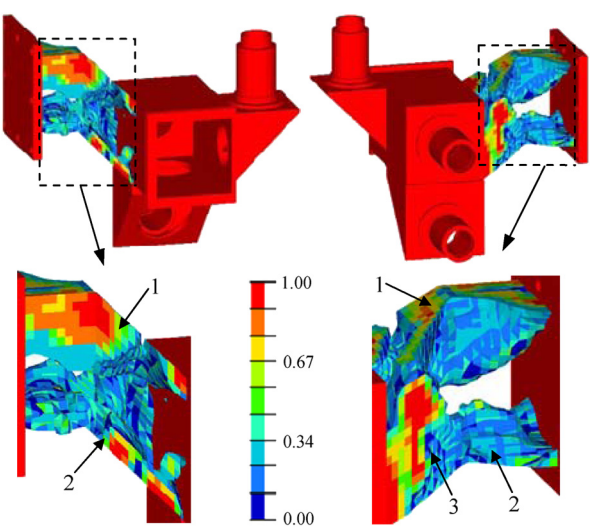

Fig. 9 Model of the topology optimization.

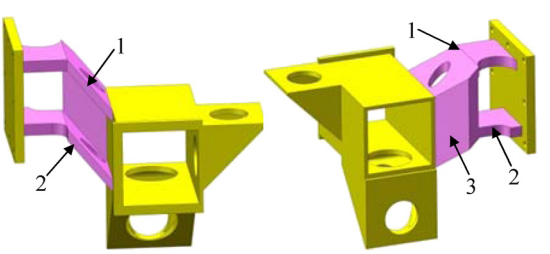

Fig. 10 New support structure extracted from the optimization model.

Table 3 Offsets of endpoints and deflection angles.

		Original structure	Optimization structure
N	Δx_N	−1.24566	−0.746639
	Δy_N	−3.90588	−2.52466
	Δz_N	−0.33600	1.25000
R	Δx_R	−1.81117	0.30061
	Δy_R	−5.47783	−2.88652
	Δz_R	−0.300000	1.30000
G	Δx_G	−5.57407	−2.44480
	Δy_G	−4.00000	−2.60000
	Δz_G	1.08700	1.19400
B	Δx_B	−6.31938	−1.56858
	Δy_B	−5.90000	−3.50000
	Δz_B	1.10000	1.20000
U	Δx_U	1.10000	−1.80000
	Δy_U	−5.60000	−4.00000
	Δz_U	−1.40000	2.40000
V	Δx_V	3.80000	−0.80000
	Δy_V	−5.60000	−4.10000
	Δz_V	−2.40000	2.60000
P	Δx_P	−2.80944	−2.65237
	Δy_P	−2.88000	−2.70000
	Δz_P	4.60000	1.20000
Q	Δx_Q	−7.03714	−4.03083
	Δy_Q	−4.03000	−2.63000
	Δz_Q	1.78245	1.40288
K	Δx_K	1.10000	−1.80000
	Δy_K	−6.83000	−4.50000
	Δz_K	−1.60000	0.30000
H	Δx_H	−1.200000	−2.70000
	Δy_H	−4.53000	−3.60000
	Δz_H	−0.400000	1.80000
	δ_1	27.6″	10.2″
	δ_2	35.3″	13.4″

Note: Units, μm. $l_1 = 50$ mm, $l_2 = 47.5$ mm, $l_3 = 52$ mm, $l_4 = 74$ mm, $l_5 = 65$ mm.

regular. Considering aesthetics and symmetry, as well as stiffness and machinability, the thicknesses of the three plates are unified by decreasing the thickness of plate 1 and increasing the thickness of plates 2 and 3. Then, a new optimization structure is extracted on the basis of preserving the main features and removing small unimportant features, as shown in Fig. 10. Compared with the original structure, which consists of two vertical plates and forms an open structure, the modifications are apparent.

6 Comparative Analysis

In this section, we provide a comparative analysis between the optimization structure and the original structure by FEA under the same weight conditions. The offsets of endpoints and the deflection angles under these two circumstances are listed in Table 3. It can be seen that with the optimization structure, the deflection angle of the visible subsystem, δ_3, decreased by 63% and that of the UV subsystem, δ_1, decreased by 62%, as compared to the original structure.

According to the focal length ($f = 50$ mm) and the pixel size ($l = 4.65$ μm), the shift of FOV of visible and UV subsystems caused by the mechanical deformation of the optimization structure can be calculated, which is ∼0.5 and 0.7 pixels, respectively. The residual shift of FOV after optical alignment is ∼0.6 pixels (details are described in Sec. 2). Thus, the total shift of FOV is ∼1.1 and 1.3 pixels, respectively. Obviously, the optimization structure can meet the requirement.

In addition, the relative shift of FOV caused by the mechanical deformation of the original structure has been calculated in Sec. 2, which is ∼1.4 and 1.8 pixels, respectively. By adding the residual shift, the total shift of FOV is ∼2.0 and 2.4 pixels. It can be seen that the total shift of FOV is lower than that of prototype experiment, which is an average of 2.3 and 2.7 pixels. This implies that there are other potential factors that can affect the analysis and experiment results, such as errors of the finite element model, pixel position measurement, and even aberration.

7 Conclusions

In this paper, a topology optimization method with the objective of minimizing the deflection angles of the optical axes is proposed. According to geometric transformation, an objective equation based on the deflection angles of the optical axes is set up, and then the topology optimization of the support structure is completed. The iteration curve indicates that the objective function is convergent, which means the deflection angle equation has a solution. A comparative analysis of the original structure and the optimization structure shows that the deflection angles of the optical axes of the visible and UV subsystems after topology optimization decreased by 63 and 62%, respectively, which demonstrates the effectiveness of the method.

References

1. X. Zhang et al., "Dual-waveband optical design for IR adaptive system," *Proc. SPIE* **9300**, 93001D (2014).
2. R. P. Jonas and D. P. Jones, "Dual waveband optics for the visible and mid waveband infrared," *Proc. SPIE* **3061**, 388–394 (1997).
3. M. Da, M. Shilong, and M. Meng, "Dual-band co-aperture infrared optical system design for irradiance measurement," *Proc. SPIE* **9300**, 930024 (2014).

4. J. M. Topaz, D. Freiman, and I. Porat, "Dual-wavelength camera for long-range reconaissance platforms," *Proc. SPIE* **4820**, 728–735 (2003).
5. Z. Lei, Z. Lu, and H. Yuan, "Research on testing method of wide distance optical axis parallelism," *Proc. SPIE* **7283**, 72833O (2009).
6. H. Jun et al., "Study on adjustment technique of optical-axis parallelism in multibeam axes optoelectronic system," *Proc. SPIE* **7283**, 72831K (2009).
7. L. Weidong et al., "Topology optimization of support structure of telescope skin based on bit-matrix representation NSGA-II," *Chin. J. Aeronaut.* **26**(6), 1422–1429 (2013).
8. Q. Xia, M. Yu Wang, and T. Shi, "A level set method for shape and topology optimization of both structure and support of continuum structures," *Comput. Methods Appl. Mech. Eng.* **272**, 340–353 (2014).
9. J. N. Richardson, R. F. Coelho, and S. Adriaenssens, "Robust topology optimization of truss structures with random loading and material properties: a multiobjective perspective," *Comput. Struct.* **154**, 41–47 (2015).
10. G. Yinjun et al., "Topology optimization design for main support structure of a space camera," *Opt. Precision Eng.* **15**(8), 1157–1163 (2007) (in Chinese).
11. M. P. Bendsoe and O. Sigmund, *Topology Optimization: Theory, Methods and Applications*, Springer, New York (2003).
12. K.-S. Park, J. H. Lee, and S.-K. Youn, "Lightweight mirror design method using topology optimization," *Opt. Eng.* **44**(5), 053002 (2005).
13. H. Kihm and H.-S. Yan, "Design optimization of a 1-m lightweight mirror for a space telescope," *Opt. Eng.* **52**(9), 091806 (2013).
14. G. B. Arfken and H. J. Weber, *Mathematical Methods for Physicists*, World Publishing Corporation, Beijing (2006).
15. R. L. Burden and J. D. Faires, *Numerical Analysis*, 9th ed., pp. 25–26, Richard Strattan, Boston (2010).
16. S. Min, S. Nishiwaki, and N. Kikuchi, "Unified topology design of static and vibrating structures using multi-objective optimization," *Comput. Struct.* **75**, 93–116 (2000).
17. T. Y. Chen and S. C. Wu, "Multiobjective optimal topology design of structures," *Comput. Mech.* **21**(6), 483–492 (1998).
18. R. T. Marler and J. S. Arora, "Survey of multi-objective optimization methods for engineering," *Struct. Multidiscip. Optim.* **26**(6), 369–395 (2004).

Xiaohu Li received his BE in mechanical engineering and automation from the China University of Petroleum in 2007 and his ME in mechanical design from Zhejiang University in 2010. Now he is a doctoral student at the University of Chinese Academy of Sciences. He also is a principal researcher at the Changchun Institute of Optics, Fine Mechanics, and Physics. His research interests include optomechanical design and structural optimization.

Ming Xuan received his ME in Changchun Institute of Optics, Fine Mechanics and Physics in 1985. He is a professor. His research interests include opto-mechanical design and micromechanics.

Junlin Ma received his BE in mechanical engineering and automation from Harbin Institute of Technology in 2009 and his ME in mechatronic engineering from Harbin Institute of Technology in 2011. Now he is a principal researcher at the Changchun Institute of Optics, Fine Mechanics, and Physics, Chinese Academy of Sciences. His research interests include optomechanical design and structural optimization.

Liming Zheng received his BE, ME, and DE in material processing engineering from China Jilin University in 2005, 2007, and 2012, respectively. Now he is an assistant researcher at the Changchun Institute of Optics, Fine Mechanics, and Physics. His research interests include optomechanical design and virtual prototype simulation.

Qiang Sun received his PhD degree in optical engineering from Nankai University, in 2003. He is a professor at the Changchun Institute of Optics, Fine Mechanics and Physics. His research interests include optical design and infrared optics.

He Wang received his BE in Dalian University of Technology in 2007, and his ME from Dalian University of Technology in 2010. Now he is a principal researcher at the Changchun Institute of Optics, Fine Mechanics and Physics. His research interests include opto-mechanical design and control system optimization.